Electronic Supplementary Information

Surface Evolution and Reconstruction of Oxygen-abundant FePi/NiFeP Synergy in NiFe Phosphides for Efficient Water Oxidation

Mao Miao,[a] Ruizuo Hou,[a] Ruijuan Qi,[b] Ya Yan,[c*] Lan Qian Gong,[a] Kai Qi,[a] Hongfang Liu,[a] and Bao Yu Xia [a*]*

[a] *Key Laboratory of Material Chemistry for Energy Conversion and Storage (Ministry of Education), Hubei Key Laboratory of Material Chemistry and Service Failure, School of Chemistry and Chemical Engineering, Wuhan National Laboratory for Optoelectronics, Huazhong University of Science and Technology (HUST), 1037 Luoyu Road, Wuhan 430074, PR China*

[b] *School of Information Science and Technology, East China Normal University, 500 Dongchuan Road, Shanghai 200241, PR China*

[c] *School of Materials Science and Engineering, University of Shanghai for Science and Technology, 516 Jungong Road, Shanghai 200093, PR China*

**Corresponding author: rjqi@ee.ecnu.edu.cn (R.Qi); yanya@usst.edu.cn (Y. Yan); byxia@hust.edu.cn (B. Y. Xia)*

1. Materials

All chemicals were used as received. $NiCl_2 \cdot 6H_2O$, $FeCl_2 \cdot 3H_2O$, $NaH_2PO_2 \cdot H_2O$, N,N-Dimethylformamide (DMF) and KOH were purchased from *Sinopharm Chemical Reagent Co., Ltd*. IrO_2 was purchased from *Strem Chemicals, Incorporated*. DI water was obtained at 18.2 Ω.

2. Preparation

In a typical synthesis, $NiCl_2 \cdot 6H_2O$ (237.69 g mol^{-1}), $FeCl_2 \cdot 4H_2O$ (198.81 g mol^{-1}), (the total moles of $NiCl_2 \cdot 6H_2O$ and $FeCl_2 \cdot 4H_2O$ is fixed at 2 mmol with different ratio), $NaH_2PO_2 \cdot H_2O$ (1 mmol, 0.106 g) and GO solution (12 mg mL^{-1}, 5 mL) were dispersed in a mixture solvent of 10 mL DI water and 10 mL DMF. After vigorously stirring and ultrasonication for respective 30 min, the mixture was poured into Teflon-lined stainless-steel autoclave (40 mL) and maintained at 160 ℃ for 16 h. After cooling down naturally to room temperature, the black precipitates were collected by centrifuge, washed with DI water and absolute ethanol each for three times to remove the unreacted reactants and soluble impurities. Finally, the as-prepared sample was freeze dried overnight to get precursors. Then, the as-prepared precursors were transferred into quartz boat and placed in an evacuated tube furnace, annealed under reducing atmosphere (the flow ratio of Ar and H_2 was 45:5) at 500 ℃ for 4 h with a heating rate of 5 ℃ min^{-1}, followed by the slow cooling to room temperature.

3. Characterization

X-ray diffraction (XRD) patterns were obtained on a PANalytical B.V. x'pert3 powder X-ray diffractometer with Cu Kα radiation (λ=1.5405Å) at 30 kV and 20 mA from 10° to 80° with a scanning increment of 0.02°. Scanning electron microscopy (SEM) and energy-dispersive X-ray spectrometry (EDX) were conducted with a field-emission scanning electron microscope (FE-SEM, Nova NanoSEM 450) at an accelerating voltage of 10 kV. Transmission electron microscopy (TEM) and high-resolution transmission

electron microscopy (HR-TEM) images were obtained with a Tecnai G2 20 scope at an acceleration voltage of 200 kV. High-angle annular dark field (HAADF) imaging and energy-dispersive spectrometry (EDS) elemental mapping analysis were performed in scanning transmission electron microscopy (STEM) mode on an aberration-corrected FEI Titan G2 60-300 field emission transmission electron microscope, operated at 300 kV (α_{max} = ~100 mrad). All XPS spectra were collected by a monochromatic Al-Kα X-ray source (hv = 1486.6 eV, Kratos, AXIS-ULTRA DLD-600W). Inductively coupled plasma mass spectrometer (ICP-MS) were obtained from PerkinElmer ELAN DRC-e instrument.

4. Electrochemical measurement

All electrochemical measurements were performed using an AutoLab (PGSTAT302N) electrochemical workstation with a typical three electrode system at 25 ℃. Hg/HgO electrode was used as reference electrode in alkaline KOH (1.0 M, pH=13.6) electrolyte. Graphite rod was used as counter electrode. A glassy carbon electrode (GCE, diameter of 5 mm, 0.196 cm^{-2} in area) covered with catalysts was used as working electrode. Working electrode was prepared as follows: 5 mg of the as-prepared catalyst was dispersed in 500 μL of ethanol containing 0.25% Nafion, then assisted with sonication treatment for at least 30 min to get a homogenous ink, 10 μL ink was carefully dropped onto the GCE via micropipettor, and the electrode was allowed to dry at room temperature. The mass loading of the electrode was calculated to be 0.5 mg cm^{-2}. The electrolyte was O_2 gas saturated.

The as-prepared electrode was activated by 10 cycles of CV scans from -0.3 V to 0.5 V vs. RHE (or 1.2 to 1.5 V vs. RHE) with a scan rate of 100 mV/s. Linear sweep voltammograms (LSV) were recorded from 1.1 V to 1.6 V (vs. RHE) at a scan rate of 5 mV/s. All potentials were referenced to a reversible hydrogen electrode (RHE) with 90% iR correction: $E_{vs.\ RHE} = E_{vs.\ Hg/HgO} + 0.098 + 0.059pH\text{-}iR$, where the R was referred to the average ohmic resistance which was obtained from EIS measurement. Electrochemical Impedance Spectroscopy (EIS) were measured at 1.5 V (vs. RHE) with the AC voltage amplitude of 5 mV and the

frequency range from 10^5 Hz to 0.1 Hz. Cyclic voltammograms (CVs) were recorded from 1.0 V to 1.1 V (vs. RHE) at different scan rates. These CV curves within non-faradaic region centered at the open circuit potential (OCP) with a potential window of 0.1 V are recorded to estimate the double layer capacitance (C_{dl}) of the catalysts. The extended durability was characterized by chronopotentiometric test with a constant current at 10 mA cm^{-2} for 48 h.

Figures and Tables

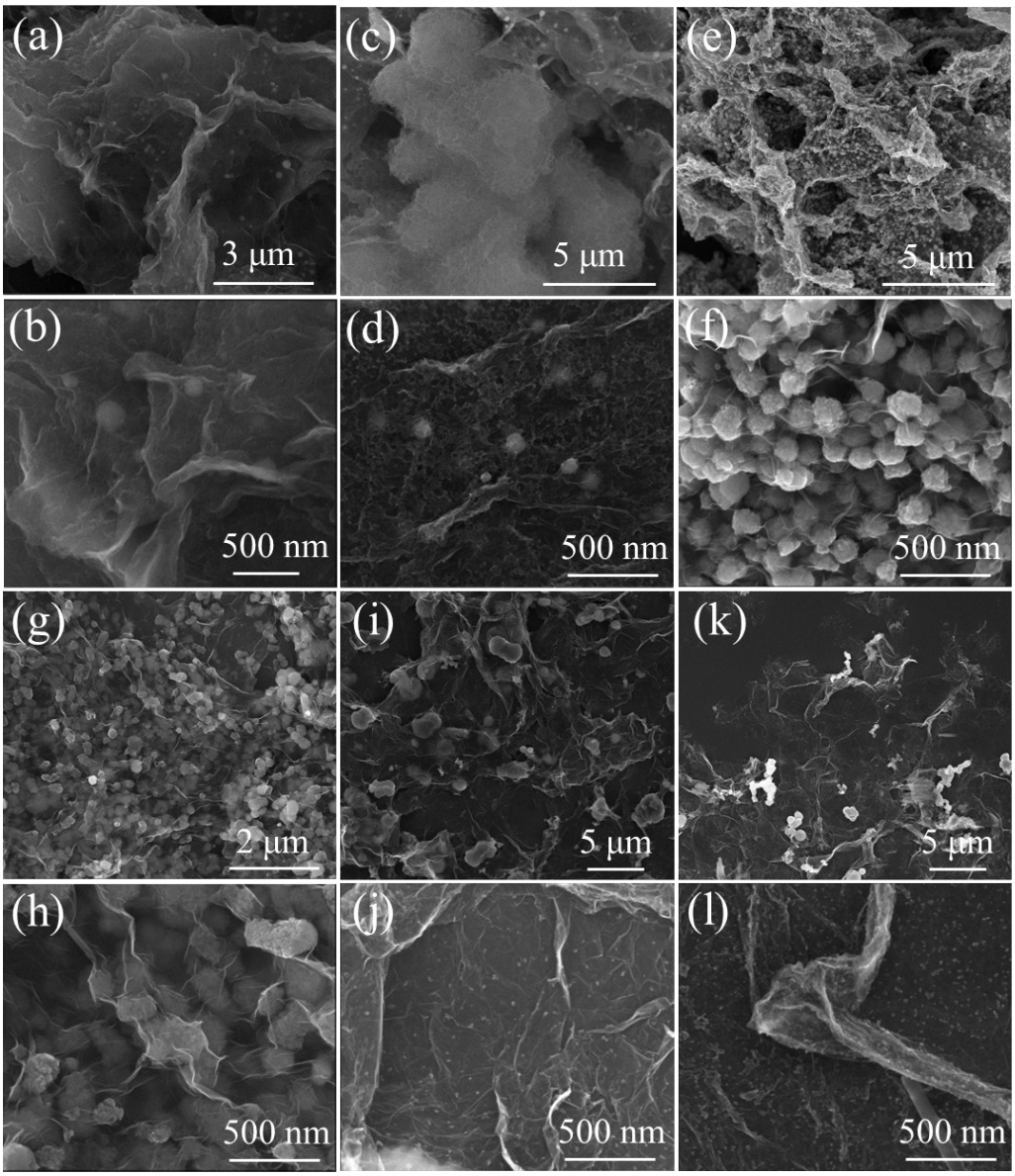

Figure S1. SEM images of hydrothermally fabricated NiFe-P@GO precursors with different ratio of Ni/Fe. (a,b) 2:0. (c,d) 1.8:0.2. (e,f)1.4:0.6. (g,h) 1:1. (i,j) 0.6:1.4. (k,l) 0:2.

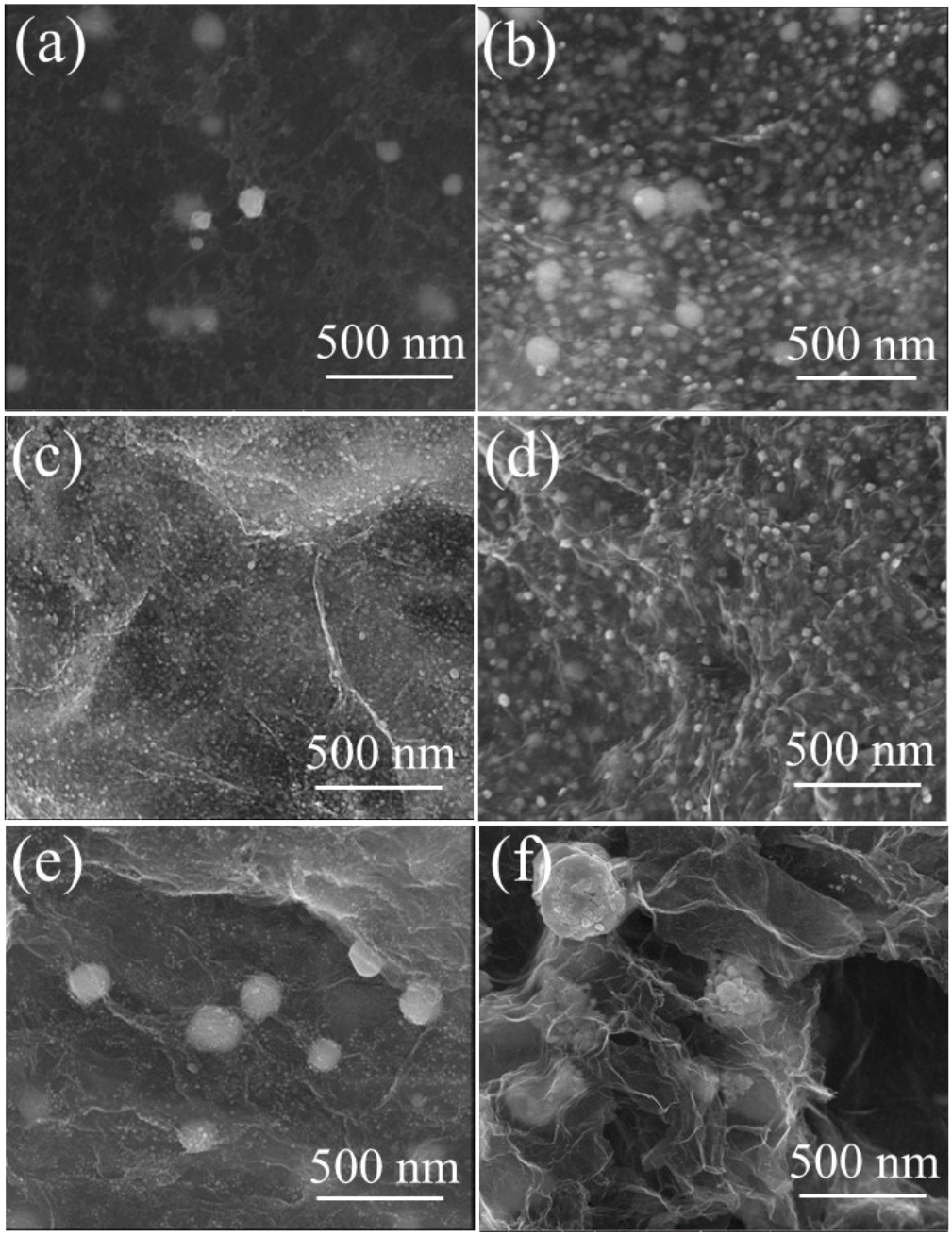

Figure S2. SEM images of annealed NiFeP@rGO. (a) 2:0. (b) 1.8:0.2. (c) 1.6:0.4. (d) 1:1. (e) 0.6:1.4. (f) 0:2.

In Figure S1-S2, the particle sizes of the as-prepared precursors with different ratio of Ni/Fe are significantly different, thereinto, the most uniform sized nanoparticles are Ni1.4Fe0.6-P@GO and Ni1Fe1-P@GO, while Ni1.4Fe0.6-P@GO is slightly smaller than Ni1Fe1-P@GO. After annealing, the trend keeps the same as in the precursors that Ni1.4Fe0.6P@rGO and Ni1Fe1P@rGO are most uniform sized among all samples and Ni1.4Fe0.6P@rGO hold smallest size. In accordance with previously reported work, the size shrinkage phenomenon is ascribe to the decomposition of precursor caused by gas emission to remove oxygen species during annealing.[1]

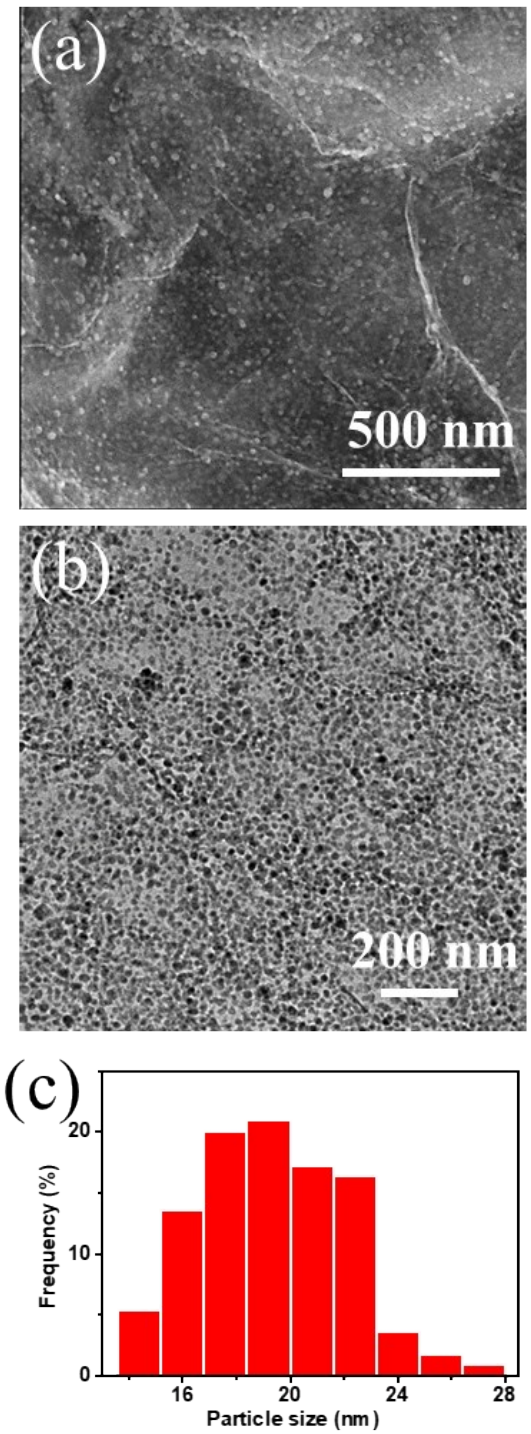

Figure S3. (a) SEM, (b) TEM images, and (c) the statistical particle size distribution of $Ni_{1.4}Fe_{0.6}P$@rGO.

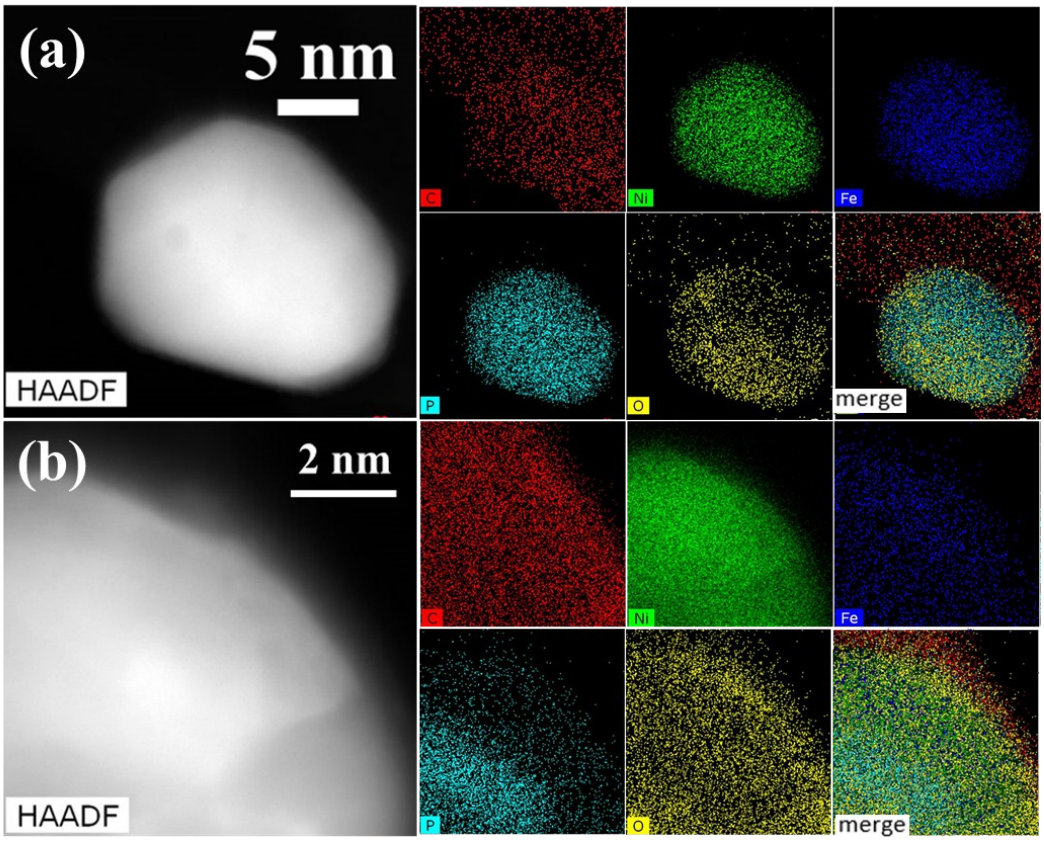

Figure S4. HAADF-STEM image and EDS elemental mapping of C, Ni, Fe, P and O of (a) single $Ni_{1.4}Fe_{0.6}P$@rGO nanoparticle, (b) periphery of activated $Ni_{1.4}Fe_{0.6}P$@rGO-a nanoparticle.

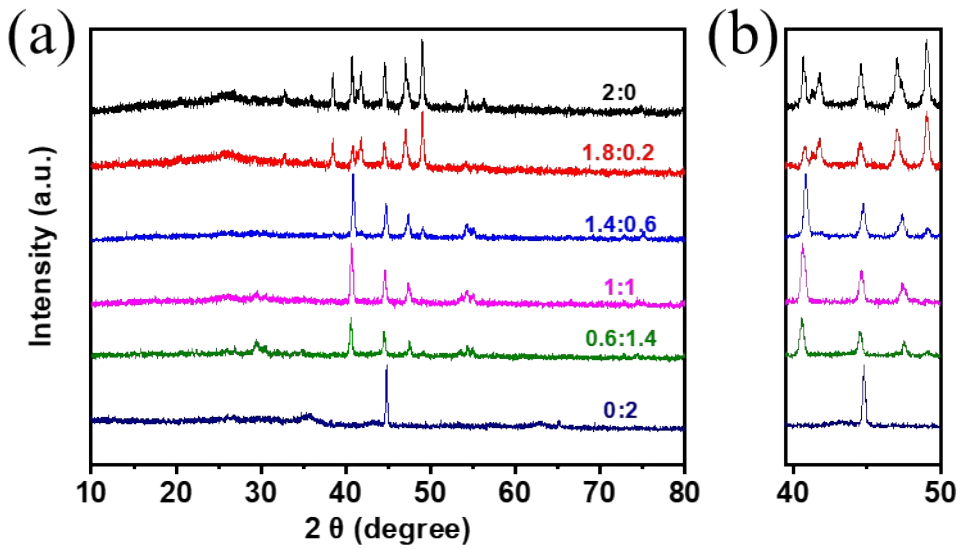

Figure S5. (a) XRD patterns of homologous materials with different Ni/Fe ratio. (b) magnified graph of (a) at 40~50 degree.

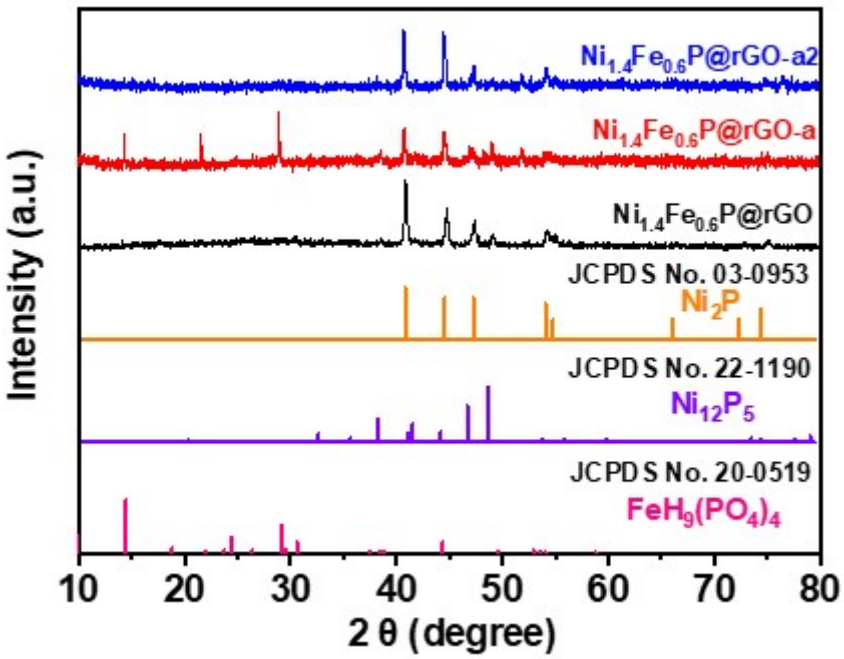

Figure S6. XRD patterns of the as parepared $Ni_{1.4}Fe_{0.6}P$@rGO and activated mateirals at different potential region. $Ni_{1.4}Fe_{0.6}P$@rGO-a (-0.3~0.5 V vs. RHE), $Ni_{1.4}Fe_{0.6}P$@rGO-a2 (1.2~1.5 V vs. RHE).

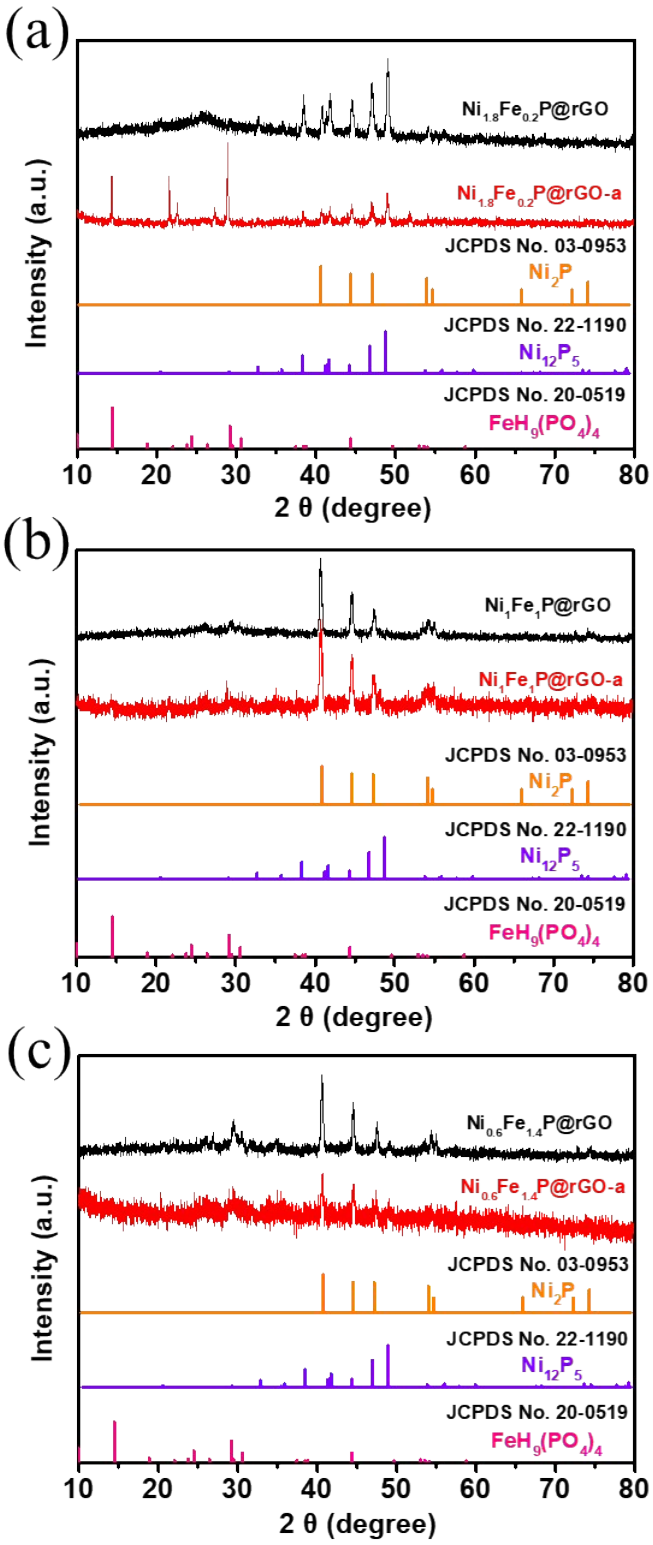

Figure S7. XRD patterns of NiFeP@rGO with different ratios of Ni: Fe before and after the activation: (a) 1.8:0.2. (b) 1:1. (c) 0.6:1.4.

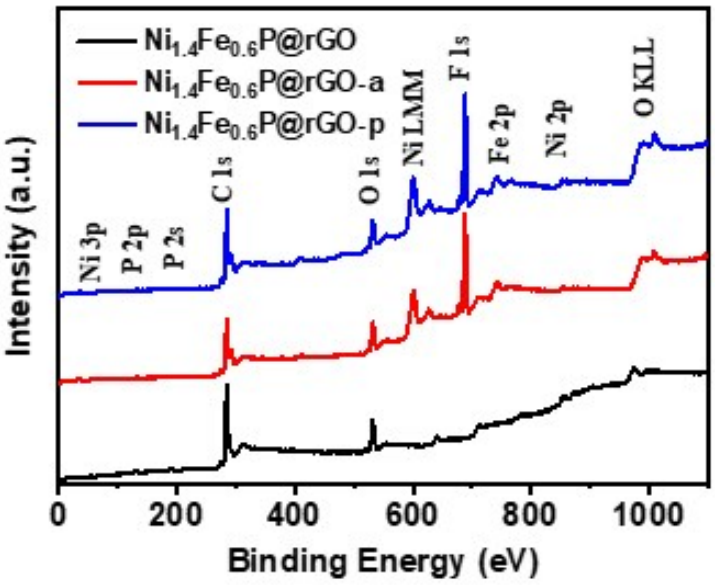

Figure S8. XPS survey spectrum of $Ni_{1.4}Fe_{0.6}P$@rGO at different stages during electrochemical test. The newly emergence of F 1s in $Ni_{1.4}Fe_{0.6}P$@rGO-a and $Ni_{1.4}Fe_{0.6}P$@rGO-p is caused by Nafion solution that containing perfluorosulfonic acid-PTFE copolymer.

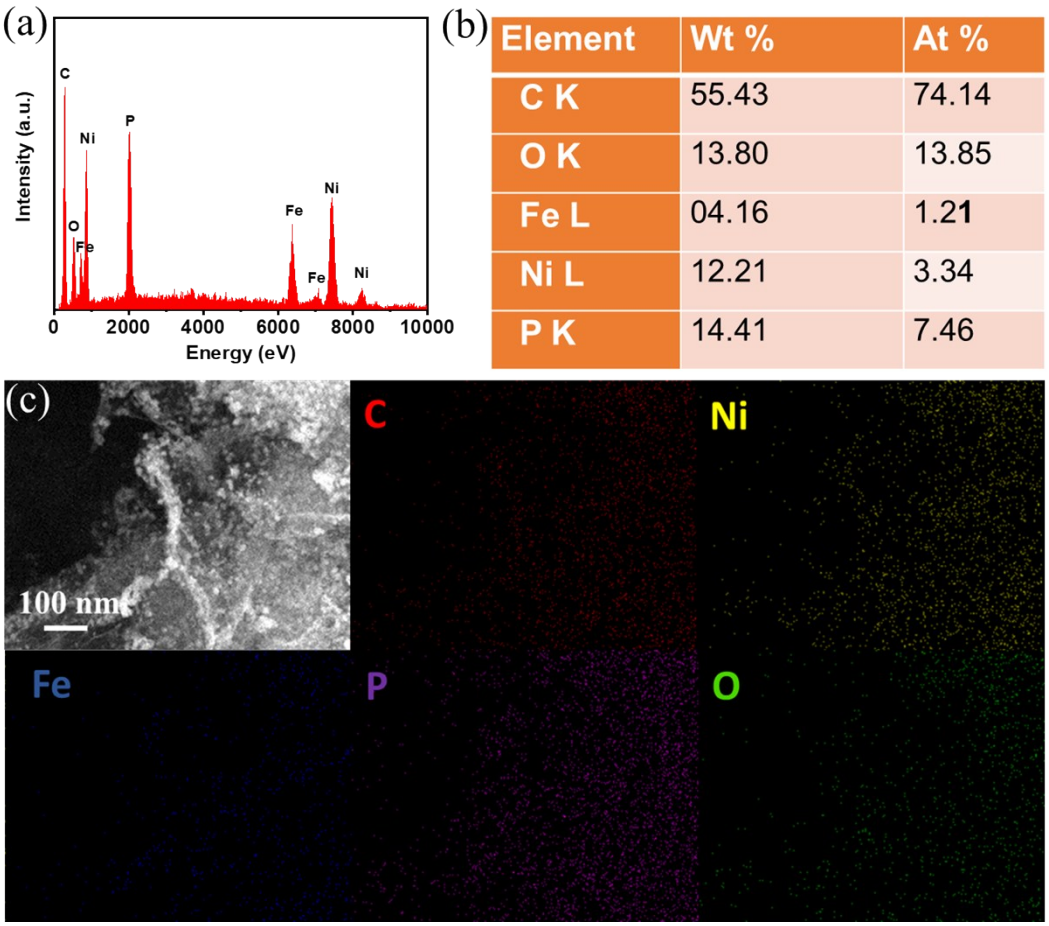

Figure S9. (a) SEM and (b) EDX elemental contents of $Ni_{1.4}Fe_{0.6}P$@rGO, (c) the elemental mapping images of C, Ni, Fe, P and O.

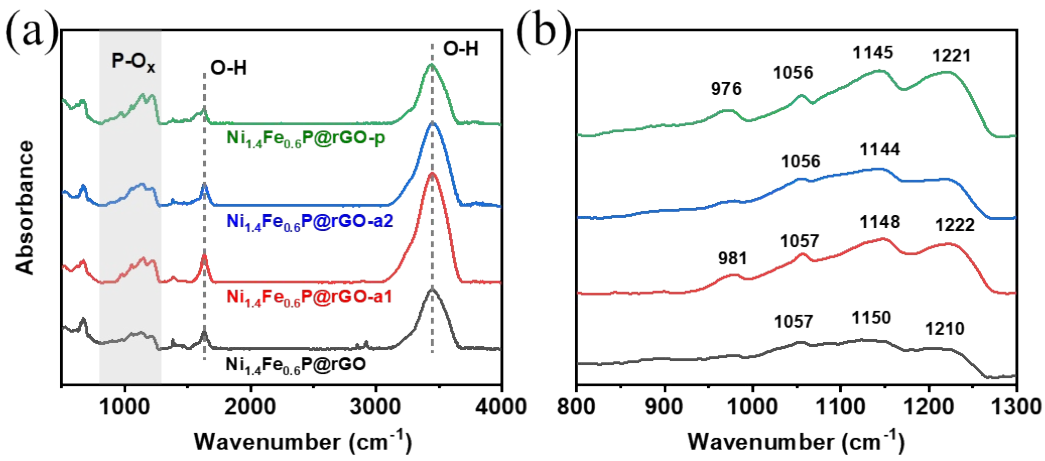

Figure S10. FTIR of $Ni_{1.4}Fe_{0.6}P$@rGO at different stages during electrochemical test. (b) is the zoom-in of the grey area in (a).

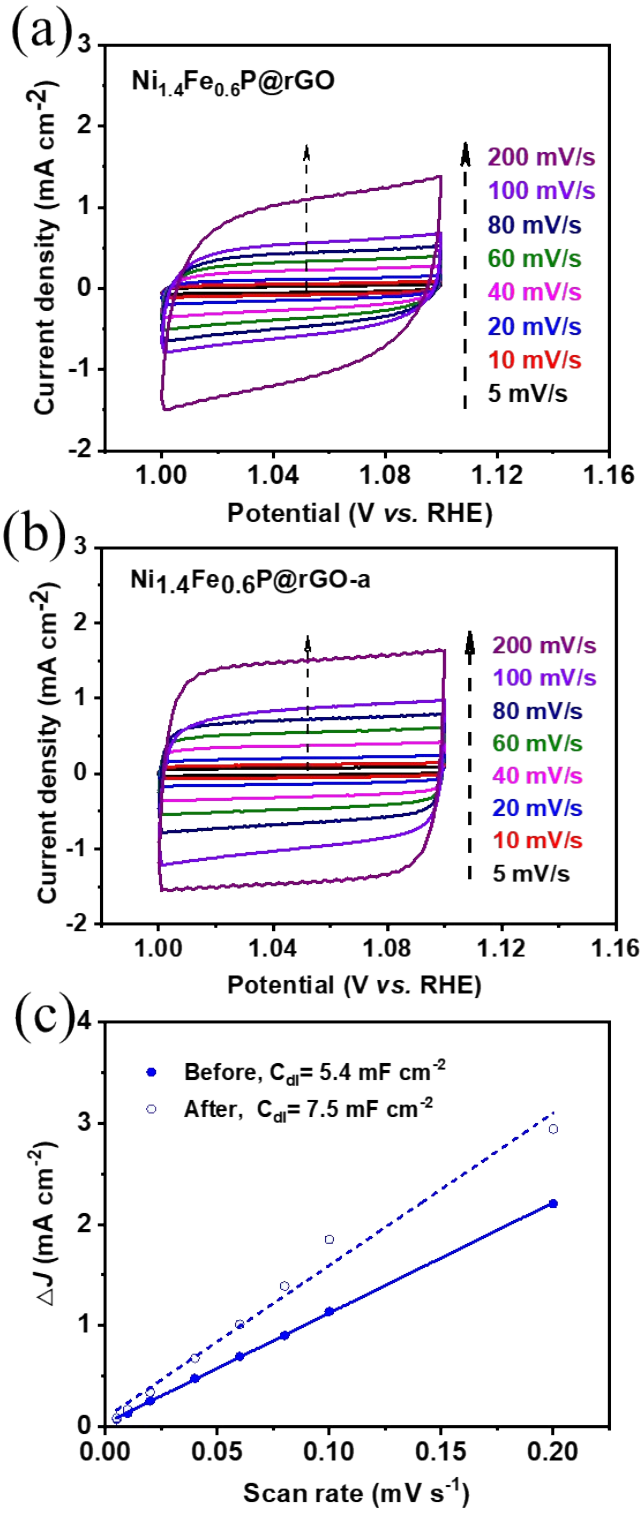

Figure S11. (a-b) Non-faradaic CV scans of various electrocatalysts at 1.0~1.1 V of $Ni_{1.4}Fe_{0.6}P$@rGO in 1.0 M KOH before and after electro-activation. (d) Capacitive currents-scan rates plots at 1.05 V vs. RHE.

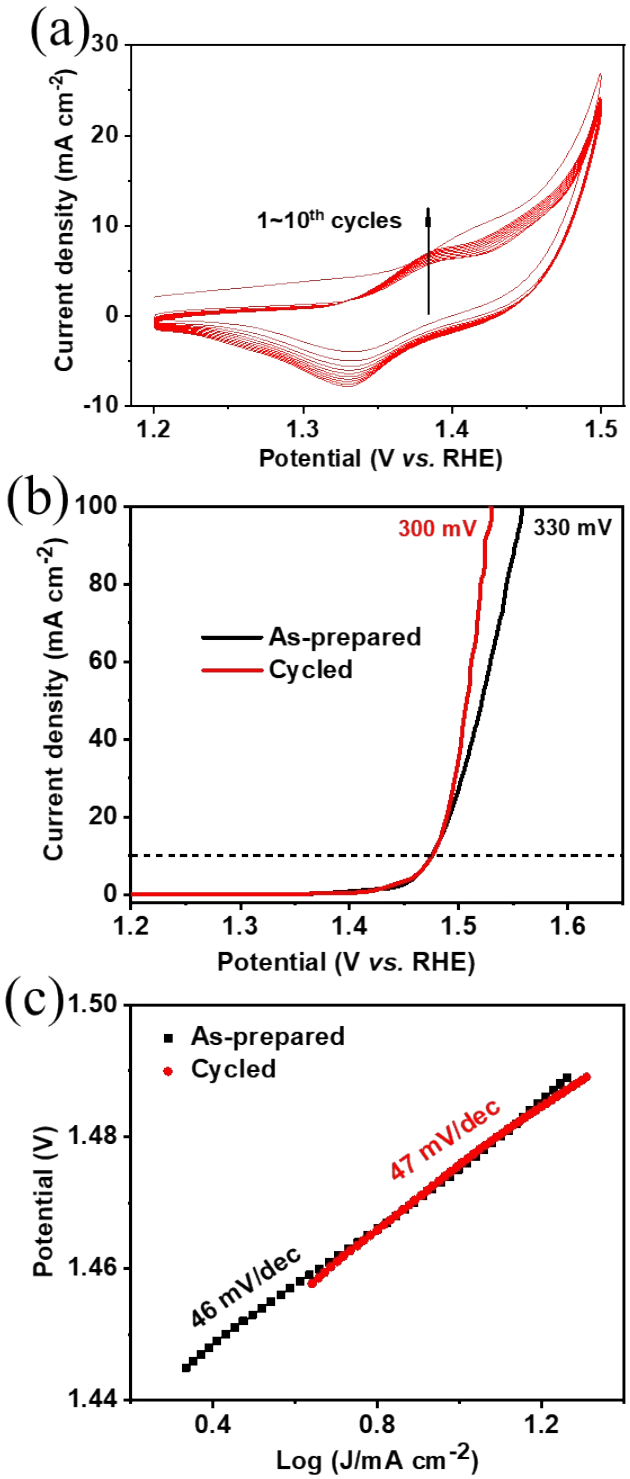

Figure S12. (a) The CV scan curves, (b) LSV curves (5 mV s^{-1}) and (c) Tafel plots of $Ni_{1.4}Fe_{0.6}P$@rGO before and after CV scans in (a).

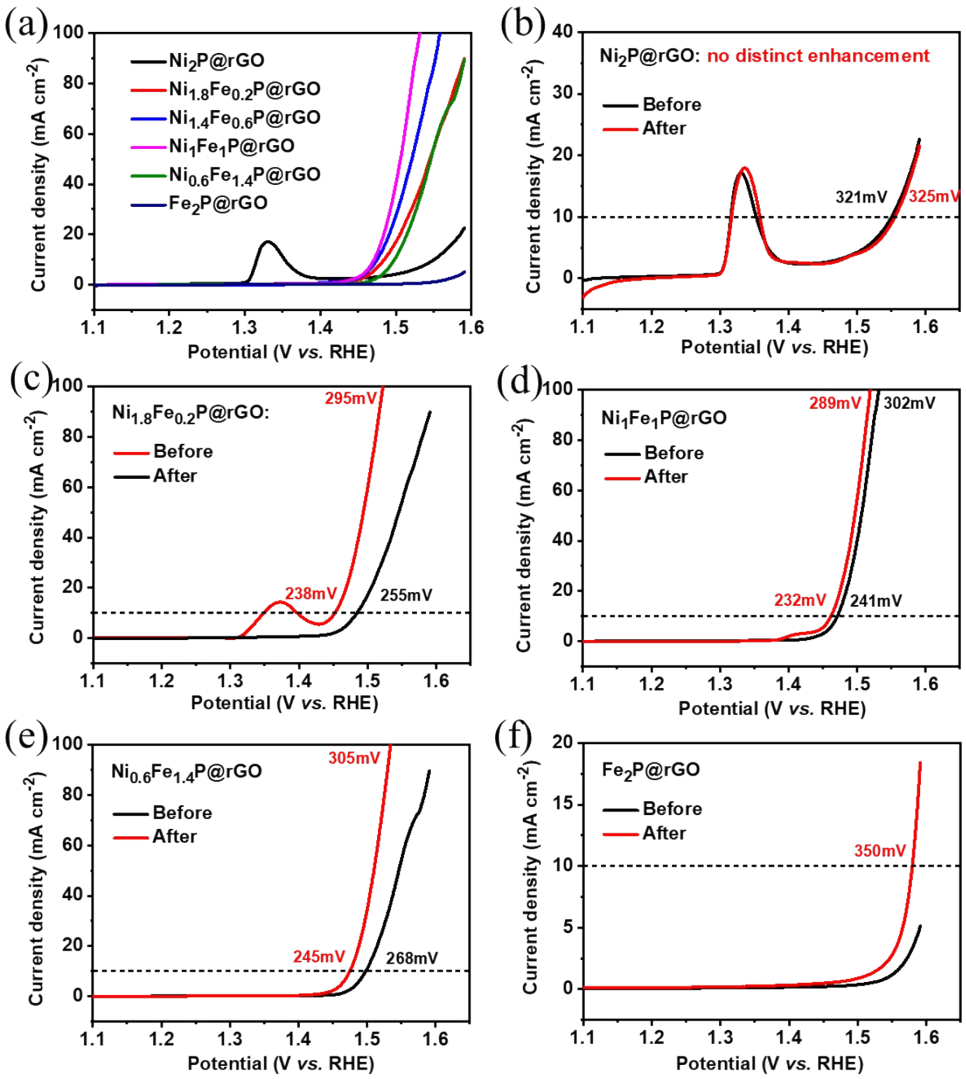

Figure S13. (a) LSV curves of as-prepared samples with different ratio. (b-f) LSV curves of the samples before and after CV scans, (b) 2:0, (c) 1.8:0.2, (d) 1:1, (e) 0.4:1.6, (f) 0:2.

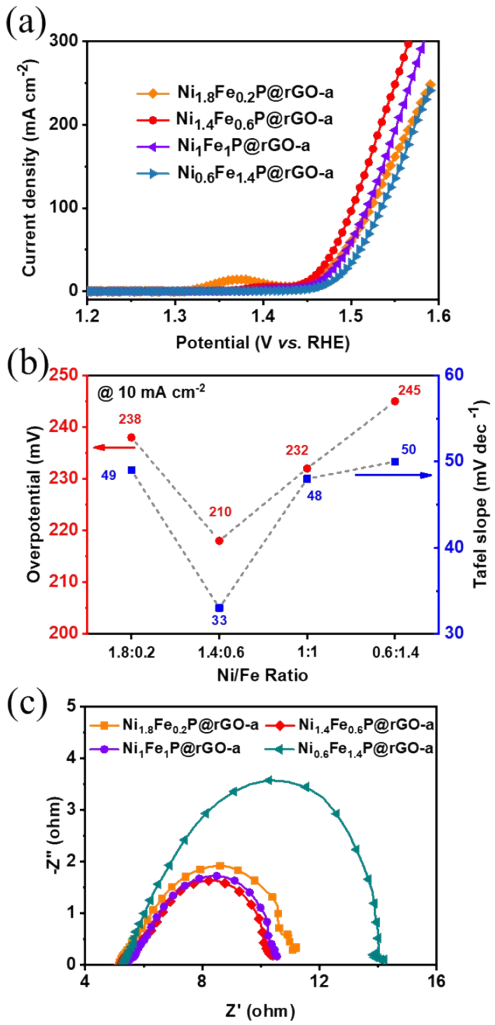

Figure S14. OER performance of homologous catalysts with different Ni/Fe ratios. (a) LSV curves, (b) the comparison of overpotential at 10 mA cm-2 and Tafel slope, (c) EIS Nyquist plots at 1.5 V (*vs.* RHE).

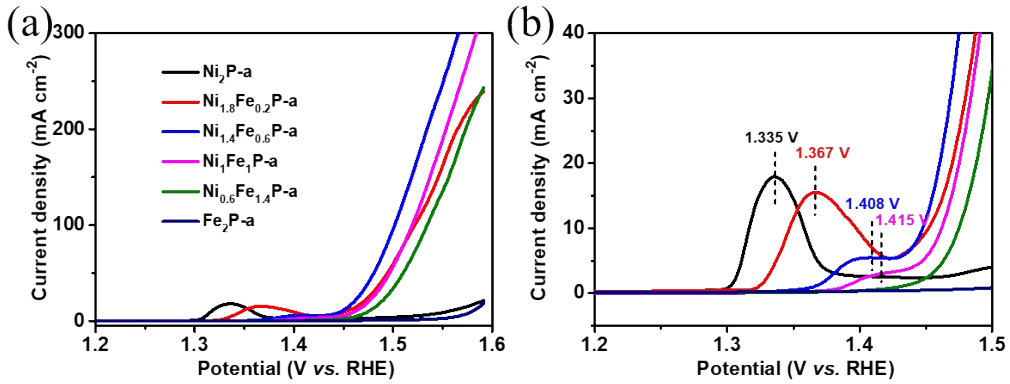

Figure S15. LSV curves of different Ni/Fe ratios after CV scans, (b) is a zoom-in of oxidation peaks of Ni^{2+}/Ni^{3+}.

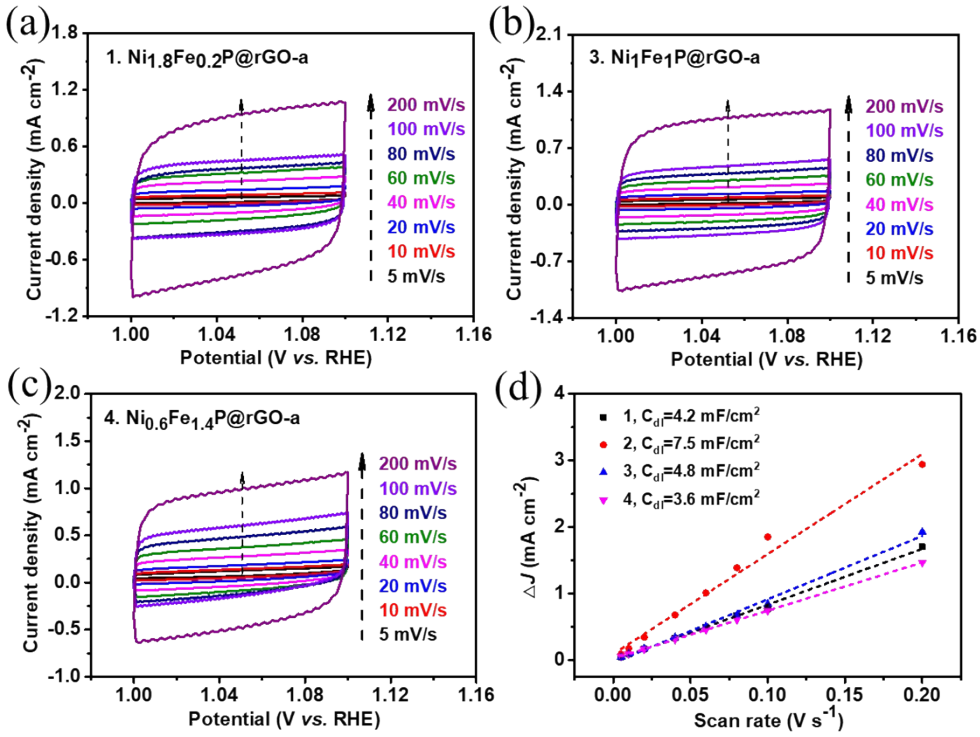

Figure S16. (a-c) Non-faradaic CV scans of various electrocatalysts at 1.0~1.1 V of various ratios of Ni:Fe. (d) Capacitive currents-scan rates plots of various electrocatalysts at 1.05 V vs. RHE.

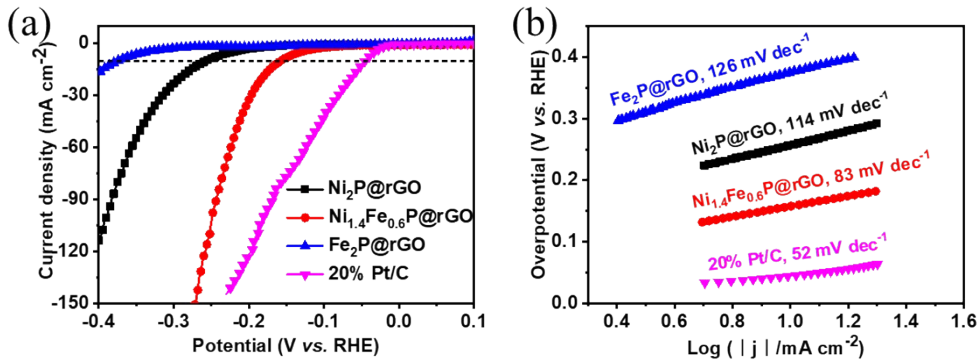

Figure S17. HER performance of various electrocatalysts. (a) LSV curves, (b) Tafel plots.

Table S1. Elemental contents (atomic ratio) of $Ni_{1.4}Fe_{0.6}P$@rGO obtained from XPS survey.

	C	O	Ni	Fe	P
$Ni_{1.4}Fe_{0.6}P$@rGO	79.05	13.89	1.04	1.33	2.93
$Ni_{1.4}Fe_{0.6}P$@rGO-a	81.3	15.86	0.92	1.19	0.73
$Ni_{1.4}Fe_{0.6}P$@rGO-p	80.85	17.24	0.89	0.81	0.21

Table S2. Elemental contents (weight ratio/atomic ratio) of $Ni_{1.4}Fe_{0.6}P$@rGO obtained from ICP-MS.

	Ni	Fe	P
$Ni_{1.4}Fe_{0.6}P$@rGO	32.75/44.54	10.72/15.34	15.58/40.12
$Ni_{1.4}Fe_{0.6}P$@rGO-a	27.13/48.88	9.82/18.61	9.53/32.51
$Ni_{1.4}Fe_{0.6}P$@rGO-p	26.65/49.41	9.56/18.64	9.1/31.95
$Ni_{1.4}Fe_{0.6}P$@rGO-immersed[1]	27.1/45.70	10.45/18.54	11.2/35.76
Electrolyte 1 (activation)	5.75	0.75	6.25
Electrolyte 2 (after stability test)	6.25	1	7
Electrolyte 3 (immersed)[2]	5.75	0.25	5

[1]the contrast sample was immersed in electrolyte for 48h.

Table S3. Comparison of typical NiFe based electrocatalysts for OER in 1.0 M KOH.

Electrocatalysts	Mass loading(mg/cm^2)	Overpotential @ 10 mA/cm^2 (η_{10}, mV)	Mass Activity @ 300 mV (A/g)	Electrolyte	Ref.
$Ni_{1.4}Fe_{0.6}P$@rGO	**0.5**	**210(η_{100}=270)**	**357**	**1.0 M KOH**	**This work**
NiFe/NF	-	η_{100}=360		1.0 M KOH	*Nat Commun* **2015**, *6*, 6616
NiFe-LDH/CNT/CFP	0.25	247		1.0 M KOH	*J. Am. Chem. Soc.* **2013**, *135*, 8452
Ni:Pi-Fe/NF	-	220		1.0 M KOH	*Chem. Mater.* **2016**, *28*, 5659
NiFeOF HF	0.785 cm^2	295		1.0 M NaOH	*ACS Catal.* **2017**, *7*, 8406
Ni-P nanoplates	0.2	300		1.0 M KOH	*Energy Environ. Sci.* **2016**, *9*, 1246
Ni_2P/rGO	0.25	260		1.0 M KOH	*J. Mater. Chem. A* **2018**, *6*, 1682
NiFeMo	1.6	238	113	1.0 M KOH	*ACS Energy Lett.* **2018**, *3*, 546
$Ni_{0.8}Fe_{0.2}O_xH_y$ film	0.1 cm^2	350@15 ± 3	140 ± 30	1.0 M KOH	*Chem. Mater.* **2017**, *29*, 120
Fe^{2+}-NiFe LDH	0.2	249		1.0 M KOH	*Angew. Chem. Int. Ed.* **2018**, *57*, 9392
$H_2PO_2^-$/NiFe LDH	0.2	240		1.0 M KOH	*Nano. Res.* 2017, *10*, 1732- 1739
NiFe LDH-GO	0.25	240		1.0 M KOH	*ACS Nano* **2015**, *9*, 1977
$Ni_xFe_{1-x}Se_2$-DO	-	195		1.0 M KOH	*Nat. Commun.* **2016**, *7*, 12324
NiFeS-2	0.25	286		0.1 M KOH	*Small* **2017**, *13*, 1700610
$FeNiS_2$ NSs	0.10	310		0.1 M KOH	*Nano Energy* **2016**, *27*, 526

References:

(1) Miao, M.; Hou, R.; Liang, Z.; Qi, R.; He, T.; Yan, Y.; Qi, K.; Liu, H.; Feng, G.; Xia, B. Y. *J. Mater. Chem. A* **2018**, *6*, 24107.